

# **SANDIA REPORT**

SAND2014-16800

Unlimited Release

Printed August 2014

## **A Comparison of Platform Options for Deep-water Floating Offshore Vertical Axis Wind Turbines: An Initial Study**

Matthew Fowler, Diana Bull, Andrew Goupee

Prepared by  
Sandia National Laboratories  
Albuquerque, New Mexico 87185 and Livermore, California 94550

Sandia National Laboratories is a multi-program laboratory managed and operated by Sandia Corporation, a wholly owned subsidiary of Lockheed Martin Corporation, for the U.S. Department of Energy's National Nuclear Security Administration under contract DE-AC04-94AL85000.

Approved for public release; further dissemination unlimited.



**Sandia National Laboratories**

Issued by Sandia National Laboratories, operated for the United States Department of Energy by Sandia Corporation.

**NOTICE:** This report was prepared as an account of work sponsored by an agency of the United States Government. Neither the United States Government, nor any agency thereof, nor any of their employees, nor any of their contractors, subcontractors, or their employees, make any warranty, express or implied, or assume any legal liability or responsibility for the accuracy, completeness, or usefulness of any information, apparatus, product, or process disclosed, or represent that its use would not infringe privately owned rights. Reference herein to any specific commercial product, process, or service by trade name, trademark, manufacturer, or otherwise, does not necessarily constitute or imply its endorsement, recommendation, or favoring by the United States Government, any agency thereof, or any of their contractors or subcontractors. The views and opinions expressed herein do not necessarily state or reflect those of the United States Government, any agency thereof, or any of their contractors.

Printed in the United States of America. This report has been reproduced directly from the best available copy.

Available to DOE and DOE contractors from

U.S. Department of Energy  
Office of Scientific and Technical Information  
P.O. Box 62  
Oak Ridge, TN 37831

Telephone: (865) 576-8401  
Facsimile: (865) 576-5728  
E-Mail: [reports@adonis.osti.gov](mailto:reports@adonis.osti.gov)  
Online ordering: <http://www.osti.gov/bridge>

Available to the public from

U.S. Department of Commerce  
National Technical Information Service  
5285 Port Royal Rd.  
Springfield, VA 22161

Telephone: (800) 553-6847  
Facsimile: (703) 605-6900  
E-Mail: [orders@ntis.fedworld.gov](mailto:orders@ntis.fedworld.gov)  
Online order: <http://www.ntis.gov/help/ordermethods.asp?loc=7-4-0#online>



SAND2014-16800  
Unlimited Release  
Printed August 2014

# **A Comparison of Platform Options for Deep-water Floating Offshore Vertical Axis Wind Turbines: An Initial Study**

Matthew Fowler, Andrew Goupee  
Department of Mechanical Engineering  
University of Maine  
35 Flagstaff Road  
Orono, Maine 04469-5793

Diana Bull  
Water Power Technologies Department  
Sandia National Laboratories  
P.O. Box 5800  
Albuquerque, New Mexico 87185-MS1124

## **Abstract**

This analysis utilizes a 5-MW VAWT topside design envelope created by Sandia National Laboratories to compare floating platform options for each turbine in the design space. The platform designs are based on two existing designs, the OC3 Hywind spar-buoy and Principal Power's WindFloat semi-submersible. These designs are scaled using Froude-scaling relationships to determine an appropriately sized spar-buoy and semi-submersible design for each topside. Both the physical size of the required platform as well as mooring configurations are considered. Results are compared with a comparable 5-MW HAWT in order to identify potential differences in the platform and mooring sizing between the VAWT and HAWT. The study shows that there is potential for cost savings due to reduced platform size requirements for the VAWT.

## **ACKNOWLEDGMENTS**

This work was funded by the US Department of Energy Wind and Water Power Technology Office.

# CONTENTS

LIST OF ABBREVIATIONS AND ACRONYMS .....	8
1. Background .....	9
1.1. Overview .....	11
1.2. Project Scope .....	13
2. Topside Design .....	14
2.1. HAWT Topside .....	14
2.2. Preliminary VAWT Topside .....	14
2.3. VAWT Topside Design Envelope .....	15
3. Platform Design .....	18
3.1. Overview .....	18
3.2. Baseline Platform Designs .....	18
3.3. Platform Design Methodology .....	19
3.4. Platform Design Results .....	22
3.5. WAMIT Analysis .....	24
4. Mooring Design .....	27
4.1. Environment .....	27
4.2. Design Procedure .....	28
4.3. Design Loads .....	29
4.3.1. Wind Loads .....	29
4.3.2. Mean Drift Loads .....	31
4.3.3. Current Induced Force .....	31
4.3.4. Dynamic Induced Loads .....	31
4.3.5. Total Mooring System Loads .....	32
4.4. Mooring System .....	36
4.4.1. Synthetic Rope .....	36
4.4.2. Clump Weight .....	36
4.4.3. Chain .....	37
4.4.4. Anchor .....	37
5. Conclusions and Future Work .....	38
6. References .....	39
Distribution .....	42

# FIGURES

Figure 1. Gross offshore wind resource for average wind speed sites over 7.0 m/s assuming one 5-MW turbine per square kilometer .....	10
Figure 2. Wind turbine substructure classes .....	11
Figure 3. Land-based wind farm, installed capital costs .....	12
Figure 4. Fixed-bottom offshore wind farm, installed capital costs .....	12
Figure 5. VAWT configurations .....	13
Figure 6. Topside CG, Pitch Moment of Inertia about CG (IPC) and Roll Moment of Inertia about CG (IRC) vs Topside Mass .....	16
Figure 7. VAWT design space as a function of topside mass .....	16

Figure 8.	a) WindFloat semi-submersible and b) Hywind spar-buoy .....	19
Figure 9.	Spar-buoy platform design results .....	23
Figure 10.	Semi-submersible platform design results .....	23
Figure 11.	Spar-buoy and semi-submersible size comparison over design range.....	24
Figure 12.	Deployment site off the coast of Maine and NBDC buoy used for wave characterization .....	27
Figure 13.	100-year contour for spectral wave conditions from NBDC buoy 44005 .....	28
Figure 14.	Taut-line mooring system with delta connection detail .....	29
Figure 15.	NREL 5-MW HAWT dimensions and drag calculation.....	30
Figure 16.	Quasi-static mooring analysis force-displacement results .....	33

## TABLES

Table 1.	HAWT topside configuration .....	14
Table 2.	Preliminary VAWT configuration .....	15
Table 3.	Functional forms for topside design envelope parameters .....	17
Table 4.	Froude scaling relationships based on mass scaling .....	20
Table 5.	Preliminary VAWT and HAWT designs .....	23
Table 6.	Environmental conditions for 100-year storm event .....	28
Table 7.	Mooring load summary.....	34
Table 8.	MARIN test data .....	35
Table 9.	Comparison of mooring model and MARIN model data .....	35
Table 10.	Mooring synthetic rope sizing .....	36
Table 11.	Mooring clump weight sizing .....	36
Table 12.	Mooring chain sizing .....	37
Table 13.	Mooring anchor sizing .....	37

## NOMENCLATURE

$A$	=	area
$BP_{req}$	=	tugboat required bollard pull
$C_D$	=	drag coefficient
CI	=	installation cost
CM	=	material cost
deg	=	degrees
$F_{aero}$	=	aerodynamic wind load
$F_{CD}$	=	current induce force
$F_D$	=	drag force
$F_{MD}$	=	mean drift force
$g$	=	acceleration due to gravity
$H_s$	=	significant wave height
Hz	=	hertz
hr	=	hour
$I_{55}$	=	combined platform and topside pitch moment of inertia
$I_{A,55}$	=	combined platform and topside pitch moment of inertia due to added mass
IPC	=	topside pitch moment of inertia about center of gravity
IRC	=	topside pitch moment of inertia about center of gravity
KC	=	Keulegan-Carpenter number
$K_{hst,55}$	=	hydrostatic stiffness
kg	=	kilogram
knot	=	knot
$L$	=	length
MHA	=	mean heal angle
m	=	meter
mt	=	metric ton
N	=	Newton
nmi	=	nautical mile
$P_{new}$	=	scaled period
$P_{orig}$	=	original period
$P_{pitch}$	=	pitch period
$R_z$	=	overturning moment lever arm
s	=	second
$T$	=	thrust force
t	=	ton
$TF_{new}$	=	scaled WAMIT transfer function
$TF_{orig}$	=	original WAMIT transfer function
$U$	=	wind velocity
$V$	=	volume
$Vel$	=	water velocity
W	=	Watt
$\lambda$	=	scale factor
$\rho$	=	density

## Unit Prefixes

$\mu$	=	micro ( $\times 10^{-6}$ )	k	=	kilo ( $\times 10^3$ )
m	=	milli ( $\times 10^{-3}$ )	M	=	mega ( $\times 10^6$ )
c	=	centi ( $\times 10^{-1}$ )	G	=	giga ( $\times 10^9$ )

## LIST OF ABBREVIATIONS AND ACRONYMS

2D	two dimensional
3D	three dimensional
AHTSV	anchor handling tug supply vessel
BL200	Bourbon Liberty 200
BOS	balance of station
CACTUS	aerodynamic analysis Code for Axial and Cross-flow TURbine Simulation
CG	center of gravity
COE	cost of energy
DCV	Deepwater Construction Vessel
DOE	department of energy
D-VAWT	Darrieus vertical-axis wind turbine
FAST	An aeroelastic computer aided engineering tool for horizontal wind turbines
FOWT	floating offshore wind turbine
GW	gigawatts
HAWT	horizontal-axis wind turbine
H-VAWT	horizontal strut vertical-axis wind turbine
MARIN	Maritime Research Institute of the Netherlands
NACA	National Advisory Committee for Aeronautics
NDBC	National Data Buoy Center
NERACOOS	Northeastern Regional Association of Coastal and Ocean Observing Systems
NREL	National Renewable Energy Laboratory
O&M	operation and maintenance
OC3	Offshore Code Comparison Collaboration
OMAE	ASME International Conference on Ocean, Offshore and Arctic Engineering
RAO	response amplitude operator
SNL	Sandia National Laboratories
SPIV	special purpose installation vessel
SWL	still water line
TLP	tension leg platform
TU Delft	Delft University of Technology
UHC	ultimate holding capacity
UMaine	University of Maine
VAWT	vertical-axis wind turbine
V-VAWT	V-shaped vertical-axis wind turbine
WAMIT	A hydrodynamic analysis code for analyzing wave/structure interaction



## **1. BACKGROUND**

When considering the wind energy potential of the United States, there is a significant contribution that can come from developing offshore wind. An estimation by the National Renewable Energy Laboratory states that the offshore wind energy resource is four times greater than the United States' current electric capacity (Musial and Ram, 2010). While there are currently no commercial offshore wind farms operation in the United States, there is considerable interest in developing this resource. Looking ahead, in order to pursue the 20% Wind Energy by 2030 scenario outlined by the United States Department of Energy (DOE), nearly 50 gigawatts (GW) of the 293GW required additional wind energy would come from offshore wind (United States Department of Energy, 2008).

There are a number of advantages offered by offshore wind compared with land based wind farms. Offshore wind sites tend to have higher wind speeds and less competition for space than onshore wind, providing an attractive incentive to use large scale turbines and wind farms.

Additionally, much of the offshore resource is located near large coastal load centers, allowing for economical transmission of energy compared with the long transmission distances required from many land based farms (Musial and Ram, 2010). For most of the highest coastal load centers along the Pacific coast and northeast United States, this offshore capacity is considered deep-water offshore as it exists in water depths greater than 60m as shown in Figure 1.

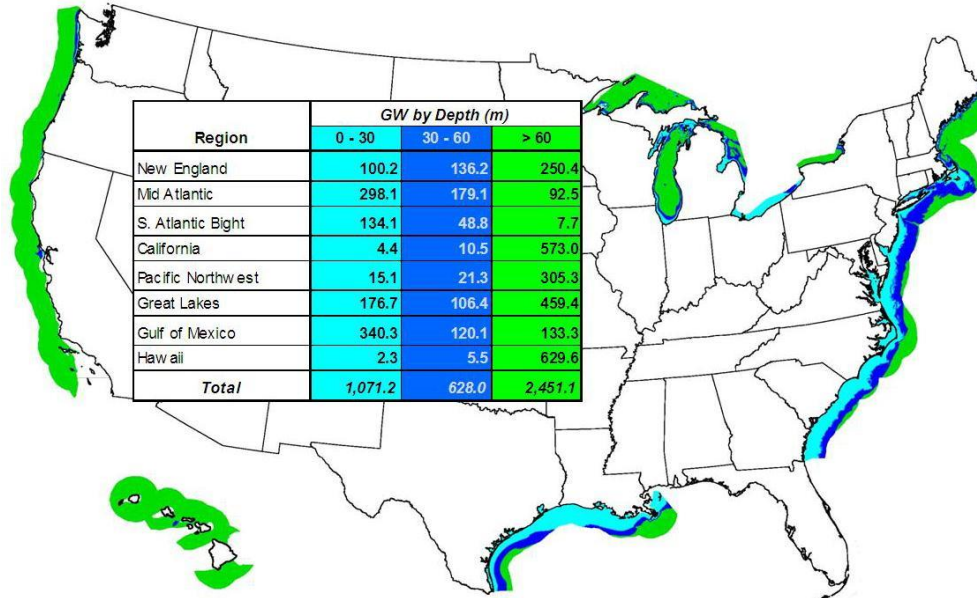


**Figure 1. Gross offshore wind resource for average wind speed sites over 7.0 m/s assuming one 5-MW turbine per square kilometer (Musial and Ram, 2010)**

This poses technical challenges for economical offshore wind farms as traditional fixed-base designs, utilized in many shallow water European offshore wind farms, are not feasible in these water depths. As water depths keep increasing, new approaches such as floating platforms become more cost effective as shown in Figure 2 (Arapogianni et al, 2013).

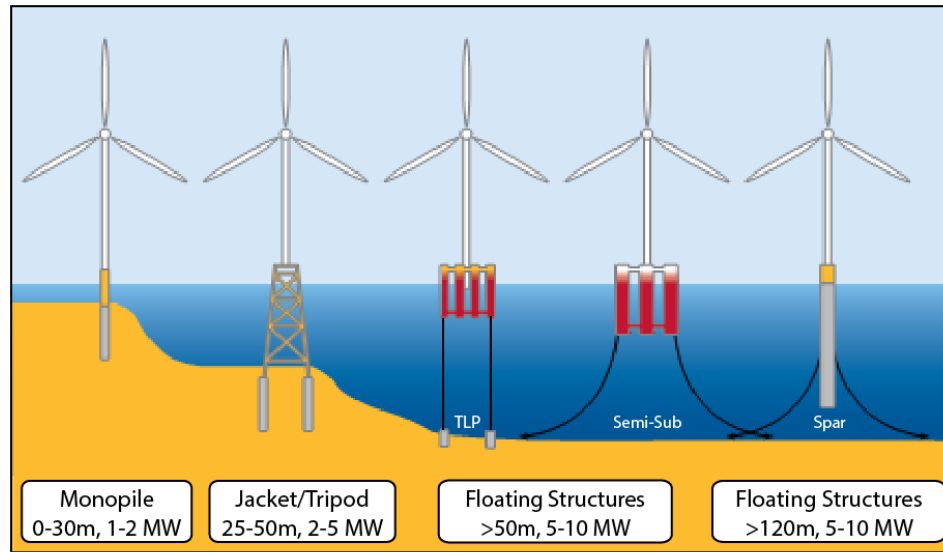


**Figure 2. Wind turbine substructure classes (Arapogianni et al, 2013)**

### 1.1. Overview

As with any new technology, the costs associated with developing a FOWT are high. Not only is the cost of the substructure significant, but the nature of the deep water offshore environment means that installation, operation, and maintenance costs are also higher than land based counterparts. The most significant capital cost associated with an offshore wind turbine farm is the balance of station (BOS) cost. An assessment by NREL estimates that while a land-based wind farm may have 23% of the total cost allocated to BOS, a fixed-bottom offshore wind farm is closer to 52% (Figure 3 and Figure 4) (Tegen et al, 2013). Methods of reducing these expenditures could greatly reduce the cost of energy (COE) for an offshore wind project. Sandia National Laboratories and its partners (TU Delft, University of Maine, Iowa State, and TPI Composites) are investigating the potential that vertical axis wind turbines (VAWTs) offer multiple advantages over other rotor configurations for reducing the BOS for offshore wind turbines. The unique arrangement of a VAWT allows the heavy generator and related components to be located at the base of the tower as opposed to the top, as is typical of a

horizontal axis wind turbine (HAWT). This configuration lowers the topside center of gravity (CG) which reduces the platform stability requirements, leading to smaller and cheaper platforms. Additionally this locates high maintenance systems close to the ocean surface thus increasing maintainability and reducing COE.

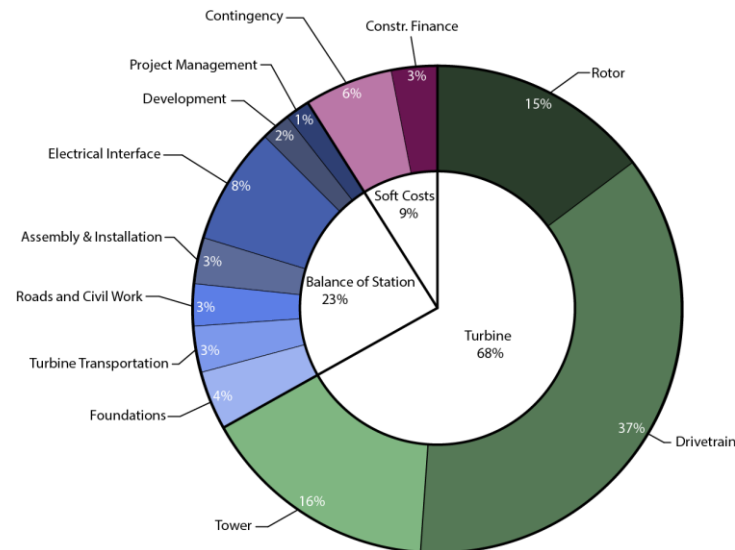


**Figure 3. Land-based wind farm, installed capital costs (Tegen et al, 2013)**

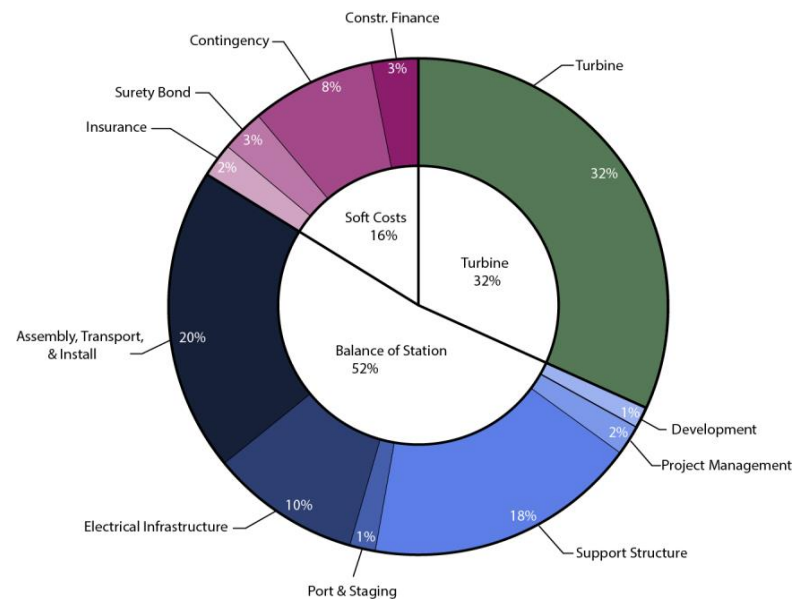


**Figure 4. Fixed-bottom offshore wind farm, installed capital costs (Tegen et al, 2013)**

## 1.2. Project Scope

The goal of this cost of energy study is to explore the costs of a 5-MW floating offshore VAWT and investigate potential BOS cost savings. To this end, a range of 5-MW VAWT topsides is determined based on Darrieus and V-VAWT designs utilizing a variety of geometries, blade materials, and strut arrangements. Figure 5 below shows various conceptual VAWT designs; from left to right Darrieus and V-VAWT rotors of 2- and 3-blades.

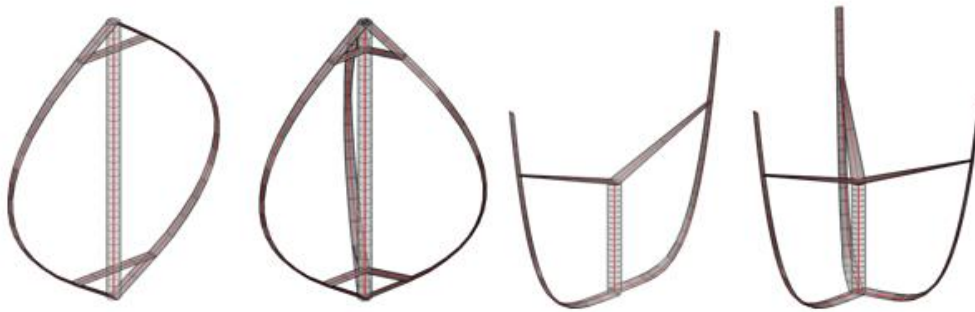


**Figure 5. VAWT rotor topside configurations**

The topside design space is parameterized by the topside mass and pertinent design characteristics are defined as functions of the topside mass where possible. Two styles of floating support platform are considered, one being a spar-buoy design similar to the Offshore Code Comparison Collaboration (OC3) Hywind spar-buoy and the other a semi-submersible similar to the WindFloat semi-submersible. For each topside in the design space, a spar-buoy and a semi-submersible platform is designed along with a mooring system. These designs are then used to determine the cost of the platform, focusing on the most significant BOS cost categories of support structure construction, mooring, system assembly, transportation, and installation. A comparable 5-MW HAWT design is also included for comparison.

## 2. TOPSIDE DESIGN

### 2.1. HAWT Topside

The topside for the HAWT comparison is based on the NREL 5-MW HAWT (Jonkman et al, 2009). The HAWT topside has a mass of 600,000 kg with a CG of 70.4m above the still water line (SWL). Note that the 600,000 kg topside mass used here is lower than the 697,500 kg specified in (Jonkman et al, 2009). This is because the original turbine was designed utilizing land-based turbines while the offshore turbine will be shorter to account for the platform freeboard and therefore lighter. For an offshore application, the tower will likely be comparable to the OC3 Hywind tower. Therefore, for the HAWT topside in this study, a tower similar to the OC3 Hywind is used, resulting in a lower mass of 600,000 kg for the turbine and tower combined (Jonkman, 2010). The primary moments of inertia in pitch and roll about the topside CG are  $5.8 \times 10^8 \text{ kg-m}^2$ . The aerodynamic thrust load is 825.0 kN with a center of pressure of 90.0m above the SWL.

**Table 1. HAWT topside configuration**

Mass (kg)	CG (m) above SWL	Roll Inertia ( $\text{kg-m}^2$ ) about CG	Pitch Inertia ( $\text{kg-}$ $\text{m}^2$ ) about CG	Aerodynamic Thrust Load (kN)	Center of Pressure (m)
600,000	70.4	$5.8 \times 10^8$	$5.8 \times 10^8$	825.0	90.0

### 2.2. Preliminary VAWT Topside

Early on in the study, characteristics of a VAWT designed for a 5-MW application were determined by scaling an existing Darrieus design. This topside wasn't optimized for use on a floating platform, but was used as a starting point for the initial platform design studies. For reference, this topside is referred to as the "preliminary VAWT" configuration and specifics are

shown in Table 2 below. This configuration is also highlighted in the overall design envelope shown in Figure 6 and Figure 7.

**Table 2. Preliminary VAWT configuration**

Mass (kg)	CG (m) above SWL	Roll Inertia (kg-m <sup>2</sup> ) about CG	Pitch Inertia (kg-m <sup>2</sup> ) about CG	Aerodynamic Thrust Load (kN)	Center of Pressure (m)
973,000	54.9	$3.77 \times 10^8$	$2.32 \times 10^9$	550.0	67.0

### 2.3. VAWT Topside Design Envelope

Once the preliminary sizing had been completed, the design envelope for the VAWT topsides was then defined by Sandia National Laboratories (Paquette, 2014) and used to define the range of topsides considered in this study. The design power for the turbine was chosen to be 5-MW and all design variations maintain this power generation capacity. While there are currently two VAWT topside designs being considered, a Darrieus (D-VAWT) and a V-VAWT, the D-VAWT design is encompassed by the V-VAWT design space in terms of the parameterizations of interest for this study (Figure 6). As such, the V-VAWT design space is used to parameterize both styles of VAWT. Based on earlier work, the key parameters that influence the floating platform design are the topside mass, center of gravity, aerodynamic load, and center of pressure. For the range of topsides considered here, the assumption is that the aerodynamic load and center of pressure remain constant over the range, but the mass, center of gravity, and primary moments of inertia about the topside CG (IPC=pitch and IRC=roll) will vary depending on the VAWT design. To parameterize the design space, the center of gravity and moments of inertia are treated as a function of the topside mass using a linear best fit (Figure 6). This allows the full range of VAWT topsides to be characterized using the topside mass as the independent variable (Figure 7 and Table 3). The circular markers on the graphs highlight the preliminary VAWT configuration. As the topside design matures, additional data on how the aerodynamic load and center of

pressure vary with topside mass could be used to parameterize these quantities in a similar manner. Additionally, more refined functional forms of the relationship between the design parameters could be established. Future work will consider a more vigorous definition of the topside design envelope utilizing more robust functional forms.

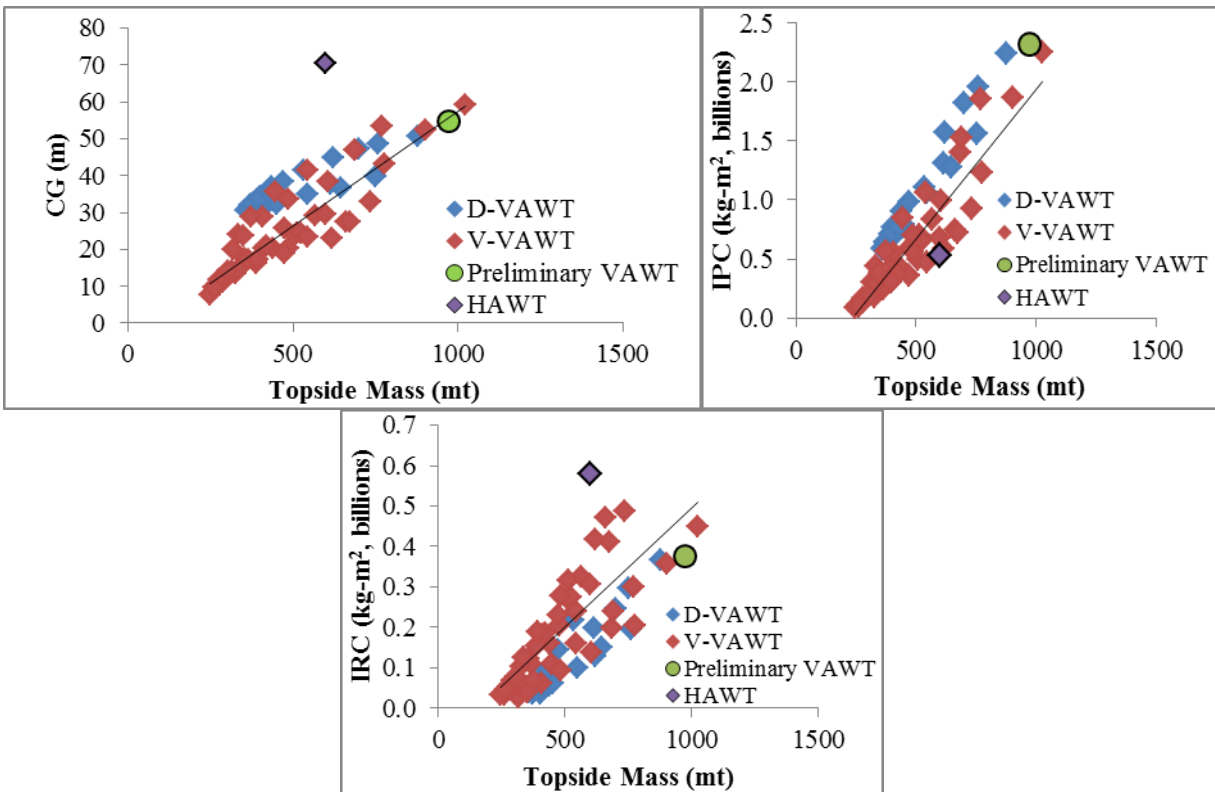


Figure 6. Topside CG, Pitch Moment of Inertia about CG (IPC) and Roll Moment of Inertia about CG (IRC) vs Topside Mass

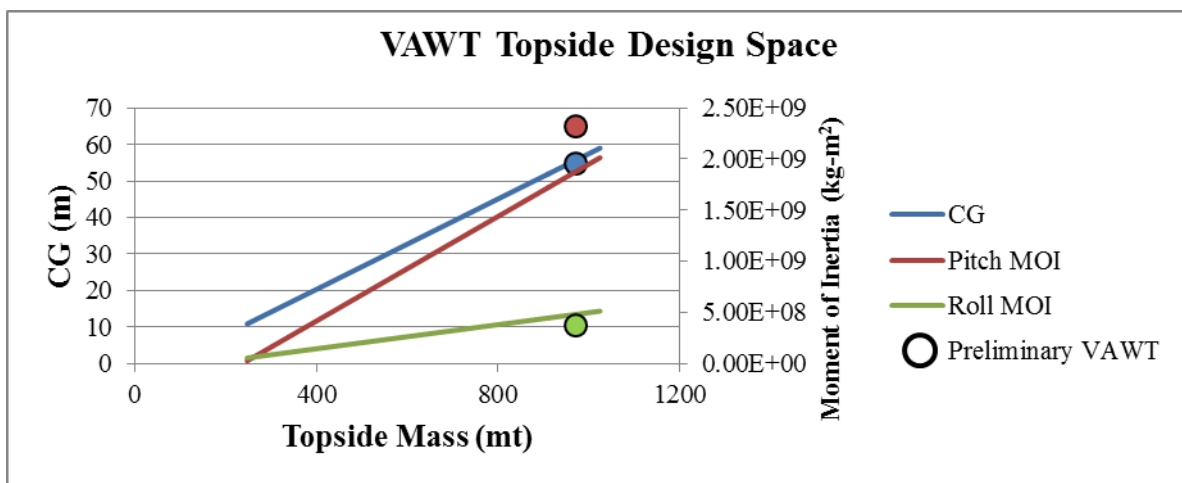


Figure 7. VAWT design space as a function of topside mass



**Table 3. Functional forms for topside design envelope parameters**

<b>Parameter</b>	<b>Functional Form</b>
Topside CG	$CG = 0.0000619401 \times \text{TopsideMass} - 4.48276$
Topside Pitch Moment of Inertia About CG	$IPC = 2557.73 \times \text{TopsideMass} - 607804000$
Topside Roll Moment of Inertia About CG	$IRC = 589.23 \times \text{TopsideMass} - 92617000$

### **3. PLATFORM DESIGN**

#### **3.1. Overview**

Designing the floating platform for an offshore wind turbine is a complicated process. As an emerging field, there is little to no historical data on floating offshore wind projects to leverage and few currently deployed systems. While experience with floating platforms designed for offshore oil and gas is applicable, the design conditions and operational requirements for a floating wind turbine are different than a floating oil production facility.

To facilitate this cost of energy analysis, two existing floating wind turbine platforms are utilized and adapted to meet the criteria of the VAWT. The baseline platform parameters are determined using a Froude number scaling approach based on achieving the desired system performance over the topside design space. The baseline platform designs are derived from existing floating platforms developed for horizontal axis wind turbines, namely the spar-buoy platform designed for use with the OC3 and DeepCwind programs and the WindFloat semi-submersible. These baseline designs are presented briefly and the scaling methods used are described. Using the topside design envelope defined above, a range of platforms are designed and the results presented. Both a spar-buoy and a semi-submersible type platform are designed for use with the VAWT topside and compared with comparable platforms designed for a HAWT.

#### **3.2. Baseline Platform Designs**

Two types of floating platform are considered, a semi-submersible and a spar-buoy. For the semi-submersible platform, a scaled 5-MW version of Principal Power's WindFloat platform is used as the baseline design. The original WindFloat is a three column semi-submersible with a draft of 23m and displacement of 7,105,000 kg (Roddier et al, 2010). The spar-buoy is based on the OC3 Hywind spar-buoy used in the OC3 study (Jonkman, 2010). The original OC3 Hywind spar-buoy was developed from Statoil's Hywind spar-buoy, which is a demonstration floating

offshore horizontal axis wind turbine on a spar-buoy and was deployed in 2009. The OC3 Hywind spar-buoy was modified from the original, due to the heavier 5-MW topside, which results in a 120m draft spar-buoy with a total platform mass (including ballast) of 7,466,330 kg (Jonkman, 2010). While both of these platforms were designed for a HAWT, they provide an appropriate initial design for a VAWT of similar capacity. Both platforms are shown in Figure 8 below.

a)



b)



**Figure 8. a) WindFloat semi-submersible (Roddier et al, 2010) and b) Hywind spar-buoy (Crome, 2010)**

### **3.3. Platform Design Methodology**

The approach for designing platforms covering the range of VAWT topsides is to apply Froude-scaling relationships to the baseline configurations described in the previous section.

Additionally, the draft of the OC3 Hywind baseline is modified from 120m to 80m due to the

100m deployment water depth of the chosen deployment site. As the end goal of this analysis is to determine the system cost, each platform is characterized by the mass of fabricated steel required as this represents the primary construction cost for the floating platform. The required mass of fabricated steel is proportional to the overall size of the platform and provides a reasonable parameter for the cost analysis. With the Froude-scaled approach, the geometry of the platform scales as the ratio of platform steel mass of the scaled design relative to the platform steel mass of the baseline design, denoted as  $\lambda_{mass}$ . This scaling relationship applies equally to each of the gross platform design parameters (draft, column diameter, etc) and has been coded into an excel spreadsheet for use in this study. The primary scaling relationships are summarized in Table 4 below.

**Table 4. Froude scaling relationships based on mass scaling**

Parameter	Scale Factor
Length (draft, spar-buoy diameter, column spacing)	$\lambda_{mass}^{1/3}$
Area	$\lambda_{mass}^{2/3}$
Platform Displacement	$\lambda_{mass}$

As described earlier, the topside design envelope is defined as a function of the topside mass. To create data for use in the sizing spreadsheet, this function is discretized at intervals of 1,000 kg of topside mass, starting at the lightest topside of 247,000 kg and ending with the heaviest at 1,025,000 kg. This results in 779 design points, each with a unique center of gravity and moments of inertia based on their mass. To adequately cover the design envelope, the sizing spreadsheet is used to design a scaled platform for each of these topside data points. This process is performed for both the spar-buoy and semi-submersible platform type. For the initial study, platforms were designed for the preliminary VAWT topside. These platform designs served as the initial platform sizing and are referred to as the preliminary platform designs. For the HAWT

design there is only a single topside data point, so only a single spar-buoy and semi-submersible platform was designed.

As described earlier, the design parameter for each platform is the required mass of fabricated steel. Due to the Froude-scaled nature of the design process, this mass is related to the design parameters of the platform as well as the dynamic and static stiffnesses of the system. By manipulating the platform fabricated steel mass, the performance of the system can be adjusted to meet the performance characteristics specified. For FOWTs, two of the most important performance characteristics are the mean heel angle due to the design wind load and the dynamics of the platform motion. For an operating turbine, the mean heel angle is limited to  $5^\circ$  to prevent loss of power generation capacity due to an excessive reduction in turbine frontal area and reduce the bending moments in the tower. To control the platform dynamics, the natural frequencies of the system need to be outside of the primary wave energy range. In this case, the pitch and roll periods are ideally between 30-40 seconds. The mean heel angle is calculated as shown in eqn. (3.1) below.

$$MHA = \frac{180}{\pi} \frac{F_{aero} \times R_z}{K_{hst,55}} \quad (3.1)$$

where  $MHA$  is the mean heel angle (in degrees),  $F_{aero}$  is the aerodynamic wind load on the turbine,  $R_z$  is the moment arm (relative to the SWL) and  $K_{hst,55}$  is the hydrostatic stiffness for pitch. The pitch period is calculated as shown in eqn. (3.2) below.

$$P_{pitch} = \frac{2\pi}{\sqrt{\frac{K_{hst,55}}{I_{55} + I_{A,55}}}} \quad (3.2)$$

where  $P_{pitch}$  is the pitch period,  $I_{55}$  is the pitch inertia, and  $I_{A,55}$  is the added pitch inertia due to added mass. Using these design conditions, an appropriately sized platform is determined for each topside in the discretized design envelope using the scaling relationships in the sizing tool.

### **3.4. Platform Design Results**

The results of the platform design are presented below. As can be seen in the graph, for the largest topsides the controlling parameter is limiting the pitch period to <40 seconds. However, as the topside mass decreases, the controlling parameter begins to shift towards keeping the mean pitch angle <5 degrees. As the topside keeps decreasing in mass, the pitch period keeps decreasing while maintaining a constant pitch angle. After a certain point, depending on the platform type, the pitch period drops below 30 seconds. At this point, there is no more design work that can be accomplished with the scaling relationships in sizing spreadsheet as decreasing the platform steel mass will lower both the pitch angle and the pitch period. Therefore, both parameters can't be satisfied once the topside becomes too light. It was chosen to maintain the pitch angle and let the pitch period continue to fall, to demonstrate the trend as shown in the regions where the pitch period drops below 30 seconds and the 5 degree pitch angle is maintained. For these light-weight topsides it is recommended that a more specialized platform design be considered instead of scaling a baseline design. Results for the preliminary VAWT design are shown with circular marks and the HAWT design is shown as diamond marks on each graphs. Additionally, the 600-mt HAWT platform was designed to have the same performance as the VAWT design in an effort to provide a similar basis for comparison. As the HAWT topside has a higher CG, larger aerodynamic load and higher center of pressure than the VAWT, the size of the platform must increase to provide a similar level of performance. This is shown in the figures below by comparing the diamond markers for the HAWT design with the design curves for the VAWT design at 600-mt topside mass.

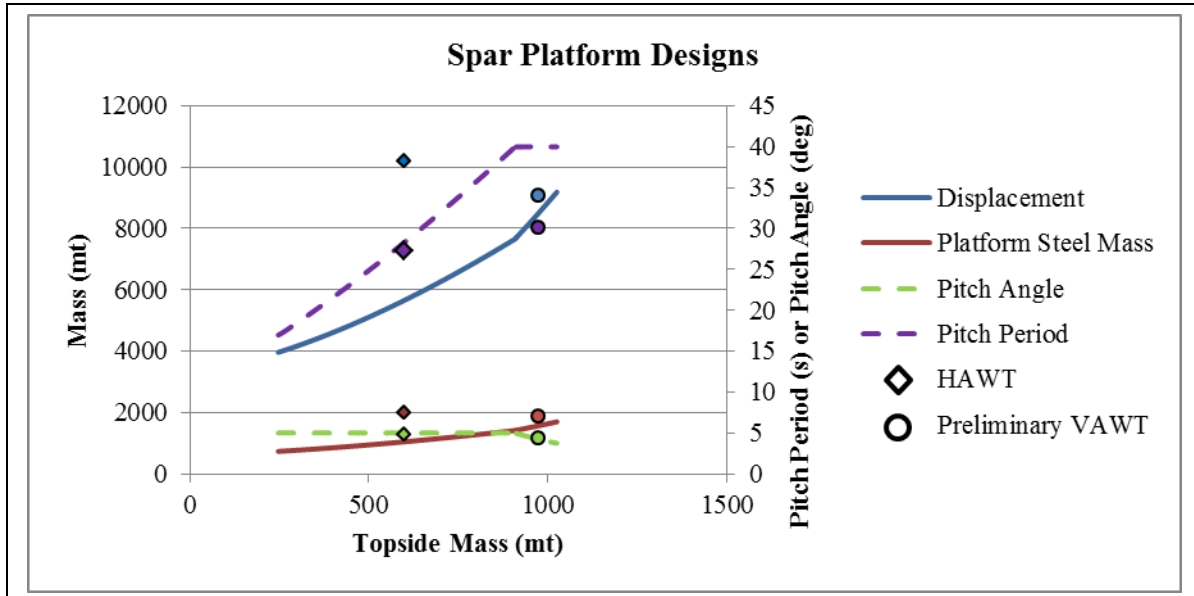


Figure 9. Spar-buoy platform design results

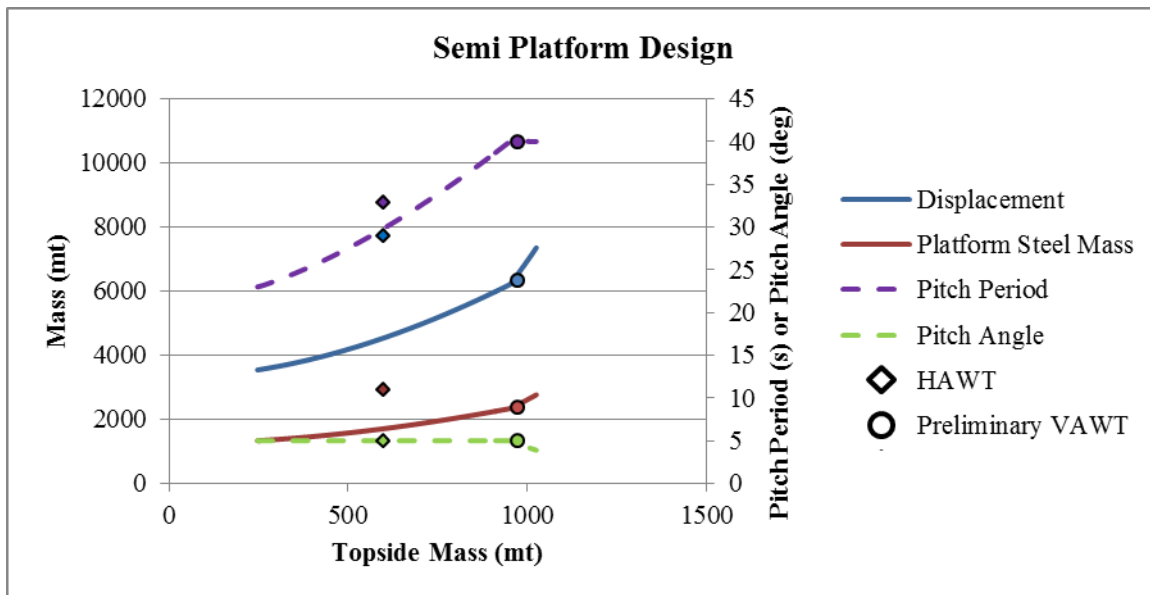
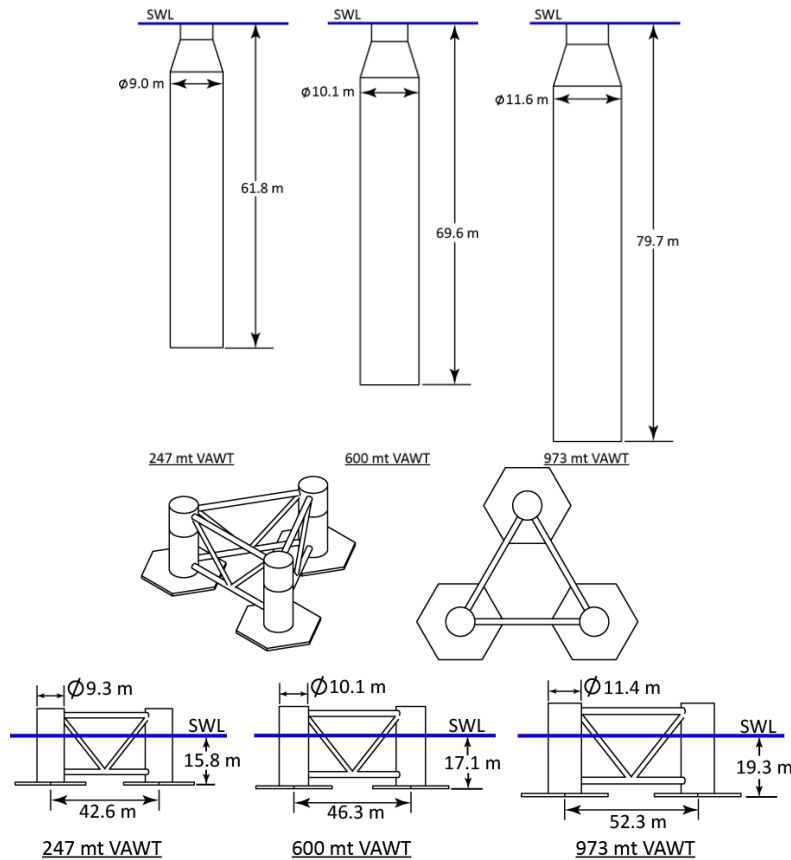


Figure 10. Semi-submersible platform design results

Table 5. Preliminary VAWT and HAWT designs

	Preliminary VAWT		HAWT	
	Spar-buoy	Semi-Sub	Spar-buoy	Semi-Sub
Topside Mass (mt)	973	973	600	600
Platform Steel Mass (mt)	1,500	2,370	2,000	2,900

A visual comparison of the scaled platforms is shown in Figure 11 for three different design points. The design points were taken to represent the range of topsides and include the 973-mt Preliminary VAWT at the upper end, a 600-mt VAWT which matches the HAWT topside mass, and a 273-mt VAWT which is the lightest VAWT topside considered. Basic dimensions are shown to illustrate the scaling relationship.



**Figure 11. Spar-buoy and semi-submersible size comparison over design range**

### 3.5. WAMIT Analysis

To determine the dynamic behavior of each platform design in the design environment, a WAMIT (WAMIT, 2011) analysis is performed on the preliminary platform for the spar-buoy and the semi-submersible. This analysis provides a baseline set of WAMIT data which can be



applied to the entire range of designed platforms by taking advantage of the Froude scaled nature of each platform.

For example, original WAMIT mean drift force results can be used to determine the mean drift force of a 90% Froude scaled platform ( $\lambda=0.9$ ) for an incident wave period of 12 seconds. First, the wave period must be scaled to account for the fact that the platform is 10% smaller than the original but the design environment is unchanged. This is calculated as

$$P_{new} = \sqrt{\frac{1}{\lambda}} \times P_{orig} \quad (3.3)$$

where  $\lambda=0.9$  is the scale factor,  $P_{orig}$  is the original period of 12 seconds and  $P_{new}$  is the scaled period. As the platform gets smaller, the new period appears larger. Another way to view this is that the wavelength of the design environment doesn't change but the characteristic length of the structure decreases, therefore the wavelength relative to the platform characteristic length appears longer.

To determine scaled results from the original WAMIT baseline data, the new period is used to lookup the desired quantity and obtain the scaled result. For the WAMIT wave diffraction force transfer function, the new transfer function ( $TF_{new}$ ) is calculated from the original ( $TF_{orig}$ ) as shown in eqn. (3.4) below.

$$TF_{new} = \frac{L}{L_o} \times \rho \times g \times A^2 \times TF_{orig} = \lambda \times \rho \times g \times A^2 \times TF_{orig} \quad (3.4)$$

The transfer is normalized by the characteristic length of the platform ( $L$ ), density of water ( $\rho$ ), gravity ( $g$ ), and the square of the wave amplitude ( $A$ ). Froude scaling of the platform changes the characteristic length, so to determine the force value one must multiply by the scaled characteristic length and the other scaling terms, which remain unchanged. As the WAMIT results were calculated originally with a characteristic length of  $L_o = 1.0$ , the scaled characteristic

length (L) is equal to the scale factor for the Froude scaled platform. This method is employed during the analysis to apply the WAMIT baseline data to the range of Froude scaled platform designs.

## 4. MOORING DESIGN

### 4.1. Environment

The hypothetical deployment site off the coast of Maine is shown in Figure 12 along with the location and water depth of a National Data Buoy Center (NBDC) buoy.

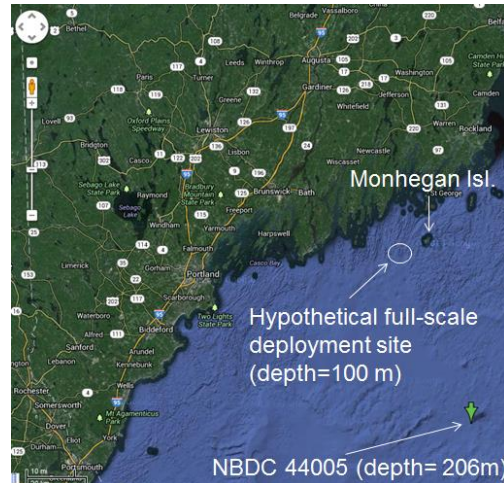


**Figure 12. Deployment site off the coast of Maine and NBDC buoy used for wave characterization**

Data from the NDBC buoy (Figure 13) was used to estimate the extreme wave conditions at the deployment site using method described by Berg (2011), noting that the 10% and 20%  $\alpha_o^2$  curves represent an “inflation” of the original contour to account for the method approximating stochastic values from a median value. There is also NERACOOS buoy E01 that is located closer to the deployment site and whose data is publicly available. The wind, wave and current conditions for these cases are shown in Table 6.

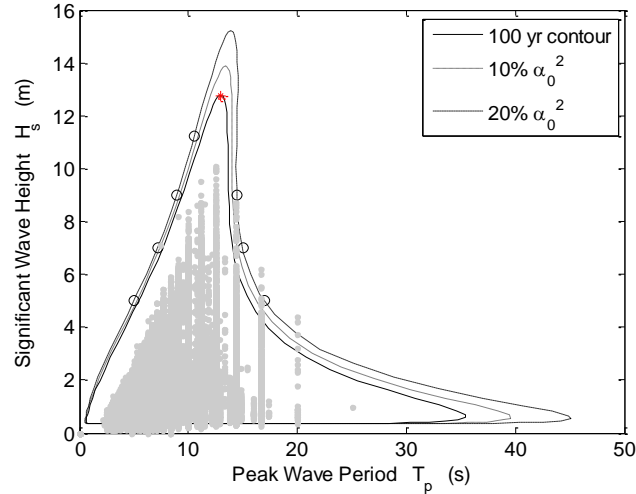


**Figure 13. 100-year contour for spectral wave conditions from NBDC buoy 44005**

**Table 6. Environmental conditions for 100-year storm event**

Quantity	Extreme Case Value
Water Depth	206 m
Regular Wave Height Equivalent	24.24 m
Period	12.97 s
Wind Speed	50 m/s
Ocean Current Speed	0.88 m/s

## 4.2. Design Procedure

The mooring system is designed as a combined synthetic rope and chain system. The synthetic rope runs in a taut configuration from the platform connection to a clumped weight at the seabed. For the spar-buoy platform, the line attaches to the platform using a delta connection to add yaw stiffness to the platform (Figure 14 inset). In the case of the semi-submersible, one line attaches directly to each platform column. For both platforms, a mooring chain runs along the seabed from the clumped weight to the anchor (Figure 14). Parameters to be chosen for this system are the mooring spread (line length, chain length), wire rope type (type, size, strength),

chain type (size, strength), clumped weight size, and the anchor type (type, size). The method for determining design forces is based on a quasi-static approach and is detailed in the next section.

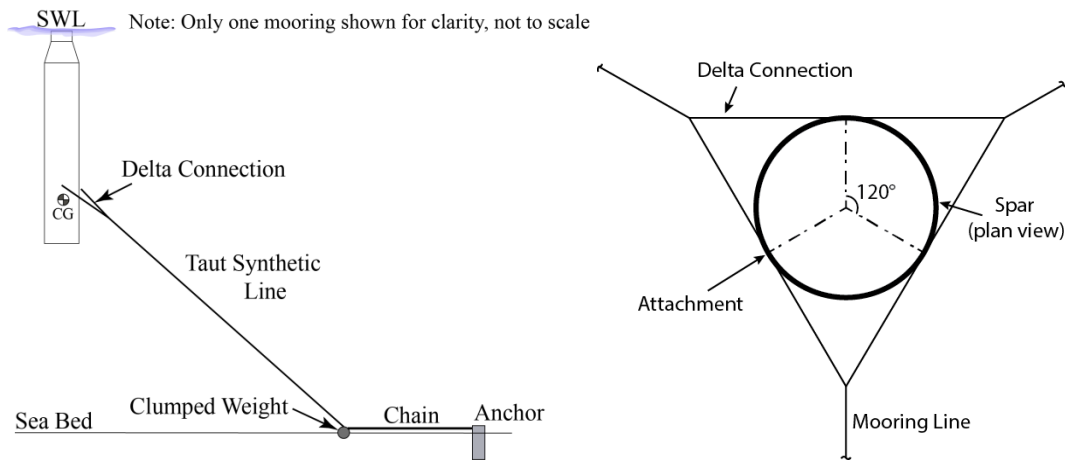


**Figure 14. Taut-line mooring system with delta connection detail**

### 4.3. Design Loads

The loads considered in this analysis can be categorized as either steady state or dynamic loads.

For the steady state loads, the dominant forces are due to wind loads, mean drift loads, and current loads. For the dynamic loads, the primary contribution is due to the platform surge motion and associated dynamic loading on the mooring system.

#### 4.3.1. Wind Loads

The wind loads are provided based on drag of the topsides in an extreme event wind case. They are considered independent of the platform type or size. For all VAWT designs, the wind load is given as 3,140 kN. This value is based on a CACTUS (Sandia National Laboratories, 2013) analysis performed by Matt Barone of Sandia National Laboratories (Barone, 2013) and represents the form drag of a parked VAWT and tower subject to the Gulf of Maine extreme mean wind speed of 50 m/s (Viselli et al, 2010). For this study it is assumed that all VAWT designs have the same cross sectional area and drag. While this assumption is likely unrealistic for the large variety of VAWT designs considered, there was not enough data available at the

time of this study to create an appropriate parameterized function. The calculated value is for what was considered the worst case VAWT design for area and drag and should be conservative. Future work will consider determining a more accurate functional relationship for the wind load based on topside size. For the HAWT, the drag loads on the turbine blades during an extreme event can be mitigated by the blade pitch mechanism. A FAST (Jonkman and Buhl, 2007) analysis of the NREL 5-MW turbine with parked and feathered blades in a 50 m/s wind yields a drag force of 90 kN. Therefore, it is chosen to use the operating thrust load of 825 kN corresponding to a wind speed of 11.4 m/s (Jonkman et al, 2009) as the worst case design wind load. The drag force on the tower and nacelle under these conditions are calculated using eqn. (4.1) below.

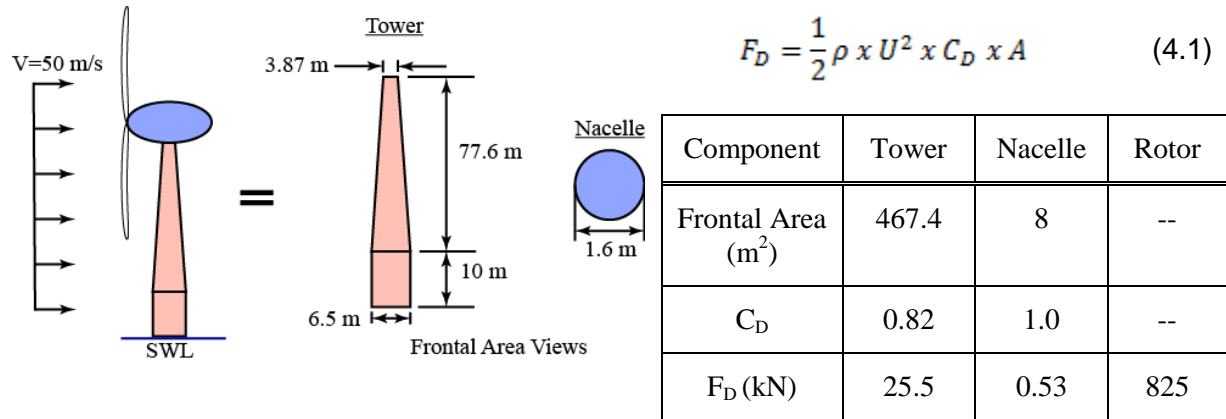


**Figure 15. NREL 5-MW HAWT dimensions and drag calculation (Jonkman et al, 2009 and Kooijman et al, 2003)**

For this analysis, dimensions of the tower are from (Jonkman et al, 2009) and the nacelle from (Kooijman et al, 2003). The drag coefficient ( $C_D$ ) of 0.82 for the tower was taken from (White, 1998) as that of a vertical cylinder with  $L/D = 87.6m/6.5m = 13.5$  and 1.0 for the nacelle is from (Kooijman et al, 2003). The drag force on the tower and nacelle are calculated using the eqn. (4.1) from White (1998), where  $A$  is the Frontal Area ( $m^2$ ) of the object,  $\rho$  is the density of air ( $1.025 \text{ kg/m}^3$ ) and  $U$  is the wind speed (11.4 m/s). The thrust value on the rotor is from (Jonkman

et al, 2009). The total worst case wind load on the HAWT is 851.0 kN which represents the operating wind load plus the drag force.

### 4.3.2. Mean Drift Loads

The mean drift loads are based on a WAMIT analysis. The force is calculated as:

$$F_{MD} = TF \times \rho \times g \times A^2 \times \left( \frac{V}{V_0} \right) \quad (4.2)$$

where  $TF$  is the adjusted period dependent transfer function from WAMIT ( $TF_{new}$  from the method described earlier for the WAMIT analysis),  $\rho$  is the density of sea water (1,025 kg/m<sup>3</sup>),  $g$  is the acceleration due to gravity (9.80665 m/s<sup>2</sup>),  $A$  is the wave amplitude (12.12 m) and  $V/V_0$  is the scaling parameter relating the initial design volume  $V_0$  to the scaled volume  $V$ . This allows the force to scale with the displacement of the platform.

### 4.3.3. Current Induced Force

The force due to the current was calculated as a function of the current velocity and the drag coefficient of a submerged cylinder. The formulation is shown below:

$$F_{CD} = \frac{1}{2} \times \rho \times A_{sub\ 0} \times C_D \times Vel^2 \times \left( \frac{A_{sub}}{A_{sub\ 0}} \right) \quad (4.3)$$

where  $C_D$  is the drag coefficient for a submerged cylinder in turbulent flow for steady current (for infinite Keulegan-Carpenter (KC) number,  $C_D = 1.05$ ),  $Vel$  is the current velocity (0.88 m/s, Viselli et al, 2010),  $A_{sub}$  and  $A_{sub\ 0}$  are the submerged areas subject to the current with the subscript  $0$  denoting the original area and  $A_{sub}$  being the scaled area. This allows the force to scale with the frontal area of the platform.

### 4.3.4. Dynamic Induced Loads

The dynamic induced mooring load is due to the dynamic surge motion of the platform. For a typical floating platform, the magnitude of the dynamic surge motion is insensitive to the mooring design as the mooring system is compliant enough to have little effect on the dynamic surge motion. From the WAMIT analysis, the dynamic surge response amplitude operator

(RAO) of the floating platform can be determined. Similar to the mean drift calculation, the range of periods for this study are based on Froude scaling the full scale period to account for the fact that the platform is changing size but the environment is not (hence the wavelength changes relative to the platform size). However, over the period range of interest, the surge RAOs for the platforms considered are a weak function of the wave period. Therefore, for the mooring analysis, the surge RAO was assumed to be constant and equal to the value for the WAMIT baseline case. A RAO value of 0.41 is used for the spar-buoy (based on WAMIT) and 0.6 for the semi-submersible (Roddier et al, 2010). Using the design wave amplitude of 12.12m, this yields a surge amplitude of 4.97m for the spar-buoy and 7.27m for the semi-submersible.

#### 4.3.5. Total Mooring System Loads

The wind, mean drift, and current forces provide a reasonable estimation of the “steady” forces acting on the platform, termed the “static load”. To this end, they are used to determine a mean surge offset of the platform in the quasi-static mooring model. The tool is based on the formulation found in (Jonkman, 2007) and computes force displacement curves based on the geometry of the mooring system and selected properties of the mooring line. To calculate the mooring forces, the method utilizes a Newton-Raphson iteration scheme to solve for the vertical and horizontal forces at the fairlead based on a given fairlead position using eqns. (4.4) and (4.5) shown below.

$$x_F = \text{Catenary} + \frac{H_F L}{EA} \quad (4.4)$$

and

$$z_F = \text{Catenary} + \frac{1}{EA} \left( V_F L - \frac{\omega L^2}{2} \right) \quad (4.5)$$

where  $x_F$  and  $z_F$  are the horizontal and vertical distances from the anchor to the fairlead,  $H_F$  and  $V_F$  are the horizontal and vertical forces at the fairlead,  $L$  is the unstretched length of the mooring



line,  $EA$  is the mooring line extensional stiffness and  $\hat{w}$  is the apparent weight in fluid per unit length of the line. The *Catenary* terms are not included here for brevity and less important for a taut synthetic mooring line system which utilizes lightweight rope and the majority of the mooring force is developed by stretching the rope. The full equations are shown in (Jonkman, 2007). Additionally, seabed friction was neglected as the taut lines are intended to not touch the seabed. Once eqns. (4.4) and (4.5) are solved, the force displacement graphs can be determined as shown in Figure 16. This figure shows how the output of the quasi-static model is used to determine the mooring forces for the system.

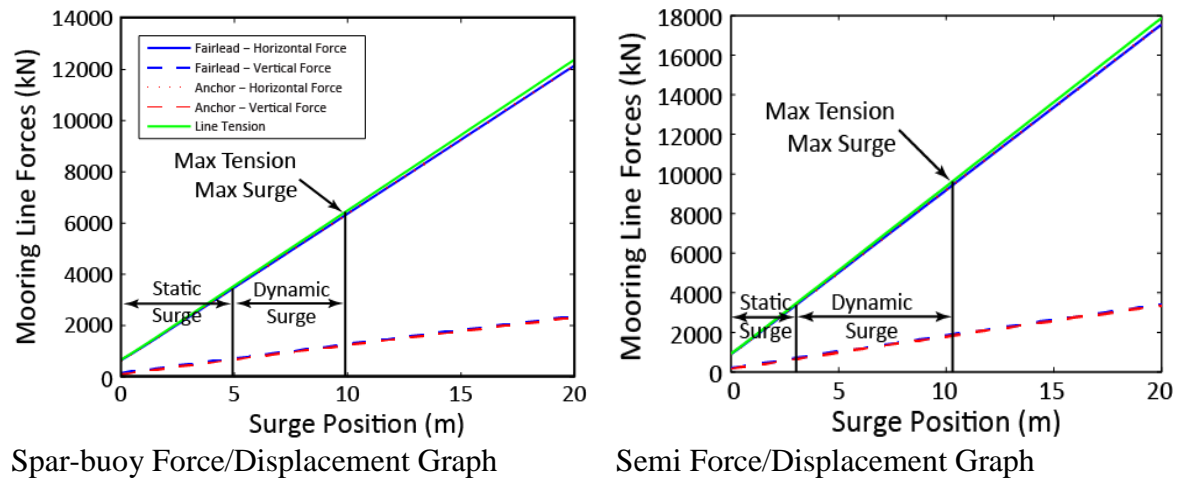


**Figure 16. Quasi-static mooring analysis force-displacement results**

First, using the quasi-static model data, the “Static Surge” displacement is determined through a reverse lookup of the static load on the platform using the “Fairlead – Horizontal Force” line as shown in Figure 16. Then, the amplitude of the “Dynamic Surge” motion of the platform is added. This gives a maximum surge displacement of the platform corresponding to the mean offset plus the maximum dynamic excursion. Using the “Line Tension” curve, the maximum mooring line tension is then determined through a reverse lookup of the maximum surge displacement. A factor of safety of 1.3 is then applied to this tension to determine the design tension in the mooring line based on the DNV recommendation for a mean tension dominated

mooring line (Det Norske Veritas, 2010). Additionally, the uplift force at the anchor is determined using the “Anchor – Vertical Force” line corresponding to the maximum surge offset. This value is used in sizing the clumped weight so that the clumped weight will be sufficiently heavy to resist the maximum vertical force, resulting in zero uplift at the anchor, as described in the following mooring sections. The mooring loads over the design range are summarized in Table 7 below.

**Table 7. Mooring load summary**

Platform	Wind Force (kN)	Mean Drift Force (kN)	Current Force (kN)	Total Static Load (kN)	Dynamic Load (kN)	Tension (1.3 Safety Factor) (kN)
VAWT Spar-buoy	3,140	5.0-14.8	231-405	3,376-3,560	~2,870	8,280-8,521
VAWT Semi	3,140	2.1-33.7	216-334	3,390-3,478	~6,052	12,517-12,634
HAWT Spar-buoy	851	16.8	436	1,304	1,434	3,634
HAWT Semi	851	23.8	296	1,171	2,100	4,340

As a qualitative check on the quasi-static methods used to determine the mooring loads, the mooring loads are compared with scale model test data from the MARIN offshore test basin. The tests performed at MARIN were part of the DeepCwind test campaign which investigated the response of three floating platforms with a HAWT topside to various wind and wave conditions using 1/50<sup>th</sup> scale models (Koo et al, 2012, Goupee et al, 2012a and Goupee et al, 2012b). The platforms considered were a spar-buoy based on the OC3 Hywind design (Jonkman and Musial, 2012), a three-columned semi-submersible, and a tension leg platform (TLP). For the purposes of this study, comparisons with the spar-buoy and semi-submersible tests are used. Of the various

load cases in the test matrix, the closest test is a white noise wave test with an  $H_s$  of 11.3m. The mooring system in the model test consists of three catenary lines arranged at  $120^\circ$  around the platform, similar to what is used in this study. During this test, a steady wind speed of 11.3 m/s generated a mean thrust on the platform of 750 kN. To compare mooring line forces, loads from the bow line are examined and shown in Table 8.

**Table 8. MARIN test data**

Platform	$H_s$ (m)	Wind Force (kN)	Total Line Load (kN)
Spar-buoy	11.3 White Noise	750	3,022
Semi	11.3 White Noise	750	9,516

To compare the results from the mooring model with the MARIN test data, the safety factor of 1.3 is removed from the calculated mooring loads. Also, as the MARIN data had a considerably lower wind force and this force is almost directly taken up by the mooring system, the difference in applied wind force is also accounted for. The results are shown in Table 9.

**Table 9. Comparison of mooring model and MARIN model data**

Platform	VAWT Mooring Model		MARIN Data		Comparison	
	Wind Load (kN)	Total Load (kN)	Wind Load (kN)	Total Load (kN)	Total Load Delta (kN)	Wind Adjusted Delta (kN)
Spar-buoy	3,140	6,555	750	3,022	3,533	1,143
Semi	3,140	9,719	750	9,516	203	-2,187

The mooring model provides a reasonable estimate of the mooring loads, considering that the MARIN data is for a different sea state and wind speed. This comparison was used to benchmark the quasi-static mooring model and ensure reasonable results for use in this study.

#### 4.4. Mooring System

Based on the previous design procedure, a mooring system was developed for the two platforms.

The overall configuration of the mooring system is similar for both platforms with the major difference being the size and/or strength of the individual components. The particulars for each platform are shown in the tables below.

##### 4.4.1. Synthetic Rope

The synthetic rope is sized based on the maximum tension determined above. This value is compared with the minimum breaking strength of synthetic polyester mooring lines designed for deep water mooring tethers of offshore platforms (WireCo, 2013) to determine the size of line required. These ropes are generally composed of multiple sub-cores which are then sheathed in a braided jacket to form a single rope. The results are summarized in Table 10 below.

**Table 10. Mooring synthetic rope sizing**

Platform Type	Max Tension (kN)	Rope OD (mm)	Stiffness (MN)	Breaking Strength (kN)
Spar-buoy	8,280-8,521	177	241	8,826
Semi	12,517-12,634	208	348	12,749

##### 4.4.2. Clump Weight

The mooring model also predicts the vertical force applied to the anchor. In this mooring design the vertical force is entirely resisted by a clumped weight to ensure only horizontal loads are resisted by the anchor. Through converting the vertical force to kg, the mass and volume of a concrete clumped weight can be determined. As with other loads in the mooring analysis, a safety factor of 1.3 was used on the vertical uplift load. Results are shown in Table 11 below.

**Table 11. Mooring clump weight sizing**

Platform Type	Max Uplift Force (kN)	Required Concrete Volume (m <sup>3</sup> )
Spar-buoy	1,573-1,619	117-120
Semi	2,392-2,414	177-179

#### 4.4.3.Chain

The chain is sized using a similar method to the synthetic line. However, instead of using the maximum tension in the line, the maximum horizontal load at the anchor is used. A safety factor of 1.3 is used for these loads as was done with the maximum tension load. The length of chain required is likely to be determined based on the topology at the installation site and will allow the anchors to be located in the best substrate. To that end, a nominal length of 100m is assumed for all platforms. Chain properties are from (Billboard Engineering, 2014). Results are shown in Table 12 below.

**Table 12. Mooring chain sizing**

Platform Type	Max Horizontal Load (kN)	Chain Type	Chain OD (mm)	Breaking Strength (kN)
Spar-buoy	8,117-8,354	R4 Stud	92	8,497
Semi	12,274-12,389	R4 Stud	114	12,420

#### 4.4.4.Anchor

The drag embedment anchor is sized based on the required horizontal tension in the mooring chain. Design charts from the Vryhoff Anchor Manual (Vryhof, 2010) were used to size an appropriate Stevpris Mk6 style drag embedment anchor based on the ultimate holding capacity (UHC) of the anchor. The design charts give UHC values based on the type of substrate and the mass of the anchor. The most conservative design line was used which corresponds to very soft clay or mud. Hence, the anchor mass is determined using the required UHC and the very soft clay design line. Results are shown in Table 13 below.

**Table 13. Mooring anchor sizing**

Platform Type	Max Horizontal Load (kN)	Anchor Mass (t)	Holding Capacity (kN)
Spar-buoy	8,117-8,354	21	8,483
Semi	12,274-12,389	31	12,455

## **5. CONCLUSIONS AND FUTURE WORK**

This study presents a comparison of floating offshore platforms designed to support a variety of VAWT configurations. Additionally, a comparable HAWT configuration is investigated to understand how the floating platforms for a VAWT compare to those for a HAWT. Results of the study show that for the chosen range of 5-MW VAWT topsides, much smaller floating platforms can be produced. When compared with the size of a comparable platform designed for a HAWT topside, the lower mass and CG of the VAWT allows for a reduction in platform size. As shown in Figure 4 earlier, one of the most significant costs of an offshore fixed-bottom wind turbine is the balance of station cost, of which a significant portion is the support structure cost. For a floating wind turbine, the support structure consists of the floating platform. Therefore, reducing the required size of the floating platform can reduce the major cost driver in the balance of station costs for an offshore wind turbine and provides motivation to pursue the VAWT design as a potentially cost effective option for offshore wind turbine applications. Future VAWT designs should focus on reducing the mass and CG of the topside, as well as lowering the aerodynamic load and center of pressure to maximize the possible reductions in platform stability requirements and cost. Additionally, methods of mitigating the wind loads during extreme events would be beneficial in reducing the loads on the mooring system, allowing for more efficient designs.

## 6. REFERENCES

1. Arapogianni, A. et al, 2013 “Deep Water - The next step for offshore wind energy,” European Wind Energy Association.
2. Barone, M., Sandia National Laboratories (personal communication December 19, 2013)
3. Berg, Jonathan C., 2011, “Extreme Ocean Wave Conditions for Northern California Wave Energy Conversion Device,” Sandia Report SAND2011-9304, Sandia National Laboratories.
4. Billboard Engineering Co. LTD., 2014, “Anchor Chain – Proof and Breaking Loads,” <[www.billboard.com.hk/file/product/pdf/4a79067d99145.pdf](http://www.billboard.com.hk/file/product/pdf/4a79067d99145.pdf)>, accessed 22 January 2014.
5. Crome, T., 2010, “Hywind Demo - Technip Experience with Offshore Wind,” Presented at the Underwater Technology Conference, Bergen, Norway, September 22, 2013, <[39](http://www.google.com/url?sa=t&rct=j&q=&esrc=s&source=web&cd=1&cad=rja&ved=0CCYQFjAA&url=http%3A%2F%2Fwww.utc.no%2Fcontent%2Fdownload%2F997%2F6325%2Fversion%2F4%2Ffile%2FUTC%2B2010%2B%2BTCR%2B-%2BHywind%2BExperience.pdf&ei=eUxaUIG4BMOzywGVnoCQCw&usg=AFQjCNFmZkYfcRh2ICXzcRv0swzFRcR_xg&sig2=m0cgMRppCRBOyRHMqayBtQ></a>>, accessed 5 December 2013.</li><li>6. Det Norske Veritas, 2010, “Offshore Standard DNV-OS-E301: Position Mooring”.</li><li>7. Goupee, A. J., Koo, B. J., Lambrakos, K. F. and Kimball, R. W., 2012, “Model Tests for Three Floating Wind Turbine Concepts,” <i>Proc. 2012 Offshore Technology Conference</i>, Houston, Texas.</li><li>8. Goupee, A. J., Koo, B., Kimball, R. W., Lambrakos, K., and Dagher, H. J., 2012, “Experimental comparison of three floating wind turbine concepts,” <i>Proc. of OMAE 2012, ASME 31st International Conference on Offshore Mechanics and Arctic Engineering</i>, Rio de Janeiro, Brazil.</li><li>9. Jonkman, J. M. and M. Buhl Jr., 2007, “Development and Verification of a Fully Coupled Simulator for Offshore Wind Turbines.” Golden, CO: National Renewable Energy Lab.</li><li>10. Jonkman, J. M. and Musial, W., 2012, “IEA Wind Task 23: Offshore Wind Technology and Deployment, Subtask 2: The Offshore Code Comparison Collaboration (OC3),” Final Technical Report.</li><li>11. Jonkman, J. M., 2007, “Dynamics Modeling and Loads Analysis of an Offshore Floating Wind Turbine” National Renewable Energy Laboratory, Technical Report NREL/TP-500-41958, NREL, Golden, CO.</li><li>12. Jonkman, J. M., 2010, “Definition of the floating system for Phase IV of OC3,” NREL Technical Report No. TP-500-47535.</li><li>13. Jonkman, J. M., Butterfield, S., Musial, W., and Scott, G., 2009, “Definition of a 5-MW Reference Wind Turbine for Offshore System Development,” National Renewable Energy Laboratory, Technical Report NREL/TP-500-38060.</li></ol></div><div data-bbox=)

14. Koo, B., Goupee, A. J., Lambrakos, K., Kimball, R. W., 2012, "Model tests for a floating wind turbine on three different floaters," *Proc. of OMAE 2012, ASME 31st International Conference on Offshore Mechanics and Arctic Engineering*, Rio de Janeiro, Brazil.
15. Kooijman, H. J. T., Lindenburg, C., Winkelaar, D., and van der Hooft, E. L., 2003, "DOWEC 6 MW Pre-Design: Aero-elastic modeling of the DOWEC 6 MW pre-design in PHATAS," DOWEC Dutch Offshore Wind Energy Converter 1997–2003 Public Reports, DOWEC 10046\_009, ECN-CX--01-135, Energy Research Center of the Netherlands, Petten, Netherlands.
16. Musial W. and Ram, B., 2010, "Large-Scale Offshore Wind Power in the United States: Assessment of Opportunities and Barriers," National Renewable Energy Laboratory Technical Report No. NREL/TP-500-40745.
17. Paquette, J., 2013, Sandia National Laboratories (personal communication November 21, 2013).
18. Roddier, D., Cermelli, C., Aubault, A. and Weinstein, A., 2010, "WindFloat: A Floating Foundation for Offshore Wind Turbines," *Journal of Renewable and Sustainable Energy* 2 033104.
19. Sandia National Laboratories, 2013, CACTUS: Code for Axial and Cross-flow Turbine Simulation [Software], <[http://energy.sandia.gov/?page\\_id=16698](http://energy.sandia.gov/?page_id=16698)>, accessed 3 January 2014.
20. Tegen, S. et al, 2013, "2011 Cost of Wind Energy Review," National Renewable Energy Laboratory Technical Report No. NREL/TP-500-56266.
21. United States Department of Energy, 2008, "20% Wind Energy by 2030," Department of Energy Report No. DOE/GO-102008-2567.
22. Viselli, A., Forristall, G. Z., Pearce, B. R., and Dagher, H. J., 2010, "Gulf of Maine Extreme Wave and Wind Design Parameters for Offshore Wind Turbines," The University of Maine.
23. Vryhof Anchors BV, 2010, "Anchor Manual 2010 – The Guide to Anchoring," Vryhof Anchors, <[www.vryhof.com/anchor\\_manual.pdf](http://www.vryhof.com/anchor_manual.pdf)>, accessed 9 December 2013.
24. WAMIT Inc., WAMIT (Version 6.4) [Software], 2011, <[www.wamit.com/index.htm](http://www.wamit.com/index.htm)>, accessed 9 December 2013.
25. White, F. M., 1998, *Fluid Mechanics, 4<sup>th</sup> Edition*. WCB McGraw-Hill, New York, NY, pp. 458-459.
26. WireCo WorldGroup: Royal Lankhorst Euronete, 2013, "Lankhorst Ropes: Ropes for Deepwater Mooring", Lankhorst Ropes, <[www.lankhorstropes.com/files/uploads/Offshore/brochures/DWM\\_brochure\\_\\_100dpi\\_\\_April\\_2013.pdf](http://www.lankhorstropes.com/files/uploads/Offshore/brochures/DWM_brochure__100dpi__April_2013.pdf)>, accessed November 22, 2013.





## **DISTRIBUTION**

1	MS0899	Technical Library	9536 (electronic copy)
---	--------	-------------------	------------------------



